Research Article

Nanoparticle Beads of Chitosan-Ethylene Glycol Diglycidyl Ether/Fe for the Removal of Aldrin

G. García Rosales [ID],[1] P. Ávila-Pérez,[1] J.O. Reza-García,[1] A. Cabral-Prieto,[2] and E.O. Pérez-Gómez[1]

[1]*TECNM/Instituto Tecnológico de Toluca, Departamento de Posgrado, Avenida Tecnológico 100 s/n. Colonia Agrícola, Bellavista, La Virgen, Metepec 52149, Mexico*
[2]*Instituto Nacional de Investigaciones Nucleares, Carretera México-Toluca S/N, La Marquesa, Ocoyoacac, C.P. 52750, Mexico*

Correspondence should be addressed to G. García Rosales; gegaromx@yahoo.com.mx

Academic Editor: Andrea Penoni

This article reports on the preparation of iron nanoparticles (FeNPs) supported in chitosan beads (Chi-EDGE-Fe) for removing aldrin from aqueous solutions. The FeNPs and Chi-EDGE-Fe beads were characterized by means of scanning electron microscopy (SEM), transmission electron microscopy (TEM), X-ray diffraction (XRD), Fourier transform infrared (FTIR), and the Mössbauer spectroscopy (MS) techniques. TEM, XRD, and MS showed that the FeNPs had core-shell structures consisting of a core of either Fe^0 or Fe_2B and a shell of magnetite. Furthermore, SEM images showed that Chi-EDGE-Fe beads were spherical with irregular surfaces and certain degrees of roughness and porosity, whilst the sorbent mean pore size was 204 nm, and the occluded iron nanoparticles in the chitosan material had diameters of 70 nm and formed agglomerates. The sorbent beads consisted of carbon, oxygen, chlorine, aluminum, silicon, and iron according to the SEM-EDS analysis. Functional groups such as O-H, C-H, -CH$_2$, N-H, C-O, C-OH, and Fe-OH were detected in the FTIR spectra. In addition, a characteristic band appeared at about 1700 cm^{-1} after the sorption process involving aldrin. MS also showed that the iron nanoparticles in the beads probably oxidized into NPs of α-Fe$_2$O$_3$ as a result of the supporting process. The isotherm of the aldrin removal followed the Langmuir–Freundlich model and presented a maximum adsorption capacity of 74.84 mg/g, demonstrating that chitosan-Fe beads are promising sorbents for the removal of toxic pollutants in aqueous solutions.

1. Introduction

Organo-chlorine pesticides (OCPs) are used extensively in agriculture and are considered to be one of the most hazardous classes of environmental and persistent organic pollutants (POPs) [1, 2]. They are toxic to many forms of wildlife, including aquatic organisms, insects, and mammals, and they persist in aquatic environments for many years after their application [3]. Their lipophilicity and persistency can lead to their bioaccumulation and biomagnification in the fatty tissues of biological organisms and food chains [4]. As a result of the high levels found in organisms, these pollutants also produce adverse effects in humans [5, 6]. Aldrin, as an OCP, presents potential risks to health as an endocrine disruptor and can damage blood, kidneys, the liver, and the central nervous system [7, 8]. Several physical, biological, and chemical methods have been developed to remove OCPs such as bioremediation [9], photochemical oxidation, catalytic degradation [10], membrane filtration [11], and adsorption [12]. Adsorption is the most popular and promising technique due to its low cost, accessibility, excellent performance, and environmental friendliness [13]. On the contrary, in some systems, FeNPs have been found to be exceptional in the removal of contaminants as sorbents or degradation moieties. In recent years, nanocomposites involving FeNPs have been used in POP removal. The constant search for materials that exhibit adequate properties for certain applications and the development of new

technological tools has given way to nanotechnology. FeNPs have been studied for the removal of a broad variety of contaminants, such as dyes, nitrates, heavy metals, and chlorinated organic compounds [14, 15], due to their size range, larger specific surface areas, and higher densities of reactive surface sites. Iron-oxide NPs are generally formed when FeNPs are exposed to contaminants, and their removal process may consist on mechanisms such as degradation, absorption, encapsulation, and diffusion. Pure FeNPs, however, tend to agglomerate when their particle sizes overcome a critical size, resulting in a decrease in their specific surface areas and active sites for the removal of contaminants. Hence, innovative and low-cost materials, including SBA-15, carbon, resins, clays, and chitosan, have been used to control FeNPs' particle sizes and remediate this disadvantage. Due to its high contents of amino and hydroxyl functional groups, chitosan has great potential for the absorption of several compounds [16]. Chitosan is a deacetylated form of chitin, a well-known cationic polysaccharide, which is an abundantly available low-cost biopolymer and the most widespread biopolymer in nature. The free amino (NH_2) and hydroxyl (OH^-) groups in its molecular structure can serve effectively as active adsorption groups. Chitosan is nontoxic, hydrophilic, biocompatible, biodegradable, and antibacterial, resulting in diverse applications in the biomedical field, cosmetics, food, textile industries, and the environment [17]. A large number of researchers have confirmed the use of chitosan as a sorbent for the removal of organic compounds from aqueous solutions since the physical-chemical properties of chitosan can be modified via the expansion of its polymer network openings. Some studies performed with chitosan beads have shown that it has high efficiency in sorption processes. Chitosan beads have also exhibited high adsorption capacities in wastewater treatment studies [18]. Additionally, the ease with which they can be separated from effluents and the possibility of sorbent regeneration has made chitosan beads one of the most prominent materials for sorption applications. However, chitosan beads exhibit instability in solutions with pH values <4, which results in the dissolution of the material and drops in its adsorption capacity. This problem is, however, solved by a reaction of the chitosan with a cross-linking agent, which leads to the conservation of the biopolymer through the formation of bonds amongst the chitosan chains. The objective of this research is to obtain an efficient chitosan-FeNPs composite material to be used as an adsorbent for the removal of aldrin. The Langmuir and Freundlich equations were used to fit the equilibrium isotherm data in order to understand and evaluate the interaction mechanisms between the surface of the composite and the contaminant.

2. Materials and Methods

2.1. Synthesis of FeNPs.

The FeNPs were prepared via the sodium borohydride reduction method, in which ferric chloride ($FeCl_3.6H_2O$ from Merck®) was dissolved in an ethanol-water mixture (1 : 1 V) and stirred for several minutes. In addition, sodium borohydride (from Merck®) was dissolved in deionized water and subsequently added dropwise to the iron-chloride solution using a burette, accompanied by vigorous hand stirring. After the first drop of sodium borohydride solution was added, solid, black particles appeared immediately, and the remaining sodium borohydride was added to complete and accelerate the reduction process. Immediately afterward, the reacting solution was stirred for an additional 10 minutes. The vacuum filtration technique was used to separate the black iron nanoparticles from the liquid phase. Two sheets of Whatman filter papers (40 mesh) were used in this process. The solid particles were washed three times with absolute ethanol to remove all the water content. The synthesized NPs were finally dried in an oven at 323 K for 12 hours and were kept in a jar in an argon atmosphere to avoid further oxidation.

2.2. Synthesis of Chitosan-FeNPs (Chi-EDGE-Fe).

Chitosan medium molecular weight powder at 80 mesh (177 μm), with over a 90% degree of deacetylation, and acetic acid of 99.8% purity from Alimentos America and Fremont® were used. Sodium hydroxide (NaOH) with 97% purity from Chemical Reagents Meyer®, ethylene glycol diglycidyl ether (EGDE) from the Tokyo Chemical Industry, and aldrin ($C_{12}H_8Cl_6$) with 98.4% purity from Chem Service® were also used. First, 78 g of chitosan powder was placed in a 500 mL beaker and dissolved in 250 mL of a 0.4 M acetic acid solution. Next, the FeNPs were added to the mixture, which was then subjected to ultrasonic shaking for 3 minutes. Then, with the aid of a peristaltic bomb and a hypodermic needle (internal diameter 0.9 mm), 100 mL of NaOH solution (0.1 M) was added dropwise to the previous solution, and the resulting mixture was stirred for 2 hours. The resulting beads were washed with water until a pH 7-8 was reached. In order to carry out the material cross-linking process, a 7 mL chitosan bead solution plus 25 mL of deionized water and 0.1 g of EGDE were put into a two-necked flask, and the deionized was adjusted to pH = 12 with the NaOH solution (0.1 M). The resulting solution was heated at 70°C and stirred continuously at 125 rpm under an inert atmosphere of N_2 for 6 hours. At the end of the reaction, the beads were left to cool to 15°C and washed with deionized water until pH = 7 was reached. After synthetizing the Chi-EDGE-Fe beads in this manner, they were subjected to a lyophilization process in a Heto PowerDry® LL1500 apparatus at −60°C and 0.5 mbar. Finally, these beads were placed inside 15 mL vials and immersed in liquid nitrogen for 2 minutes. The samples were then placed in the equipment nozzles. The total lyophilization process took around 24 hours.

2.3. Characterization of the Materials: SEM, TEM and MS, DRX, and FTIR.

The morphological analysis was performed via a scanning electron microscope JEOL® JSM-5900LV. The solid samples were sprinkled on a metallic disk and covered with gold for 100 seconds using the AJA® sputtering system ATC 1500. The chemical composition was determined by means of the EDS system (Oxford® 7279), which included the scanning electron microscope. In order to study the morphologies and sizes of the FeNPs supported in the

chitosan beads (Chi-EDGE-Fe) via transmission electron microscopy (TEM, model JEOL® 2010), a sample was prepared by dispersing a small amount of Chi-EDGE-Fe in ethanol using an ultrasonic bath with a few drops of suspension that were then placed on a carbon film supported on a copper substrate. For the identification of the iron phases in the FeNPs and Chi-EDGE-Fe materials, approximately 50 mg of material was placed in a Lucite sample holder and MS studies were performed using a Wissel® constant acceleration spectrometer with ^{57}Co/Rh. The reported isomer shifts are referred to, as those of metallic iron. The crystal phases of FeNPs, Chi-EGDE, and Chi-EGDE-Fe were analyzed using a BRUKER® (D8 Discover) XRD diffractometer with a copper anode X-ray tube ($\lambda = 1.543$ Å); the X-ray diffraction reflections were measured in a range from 4° to 70° in 2θ° scale, utilizing a 0.02 step size and a scan speed of 1°/min. The FTIR spectra were obtained via a Scientific Nicolet® iS5 spectrometer and used to determine the functional groups in the composite material. The recorded FTIR spectra ranged from 4000 cm^{-1} to 500 cm^{-1} over the course of 50 scans.

2.4. Surface Characterization: BET, Active Site Density, and Isoelectric Point.

The surface areas of the beads were determined by using the Multipoint BET Nitrogen Adsorption technique and the BELPREP-flow II (BEL Japan® Inc.) device. Prior to analysis, the samples were degassed for 1 hour at 30°C. In order to determine the active site density, 30 mL of NaClO$_4$ solution (0.1 M) was added to a 50 mL test tube to be used as a reference or blank sample. Then, 300 mg of beads were added to another test tube containing an additional 30 mL of the blank sample. The solutions were stirred for 24 hours at room temperature. At the end of this process, the pH of the sample suspension was adjusted to a pH = 2 by means of a 0.1 M solution of HClO$_4$. Then, the suspension was readjusted to a pH = 12 via the dropwise addition of a 0.1 M solution of NaOH with a micropipette. The pH of the solution was measured using a Hanna Instruments® model HI3221 potentiometer. Finally, the active site density was calculated using the equation developed by Bell et al. [19]. In order to determine the isoelectric point, ten samples of 0.01 g, 0.02 g, 0.04 g, 0.06 g, 0.08 g, 0.10 g, 0.20 g, 0.40 g, and 0.50 g in 10 mL of deionized water were placed in 15 mL centrifuge tubes and centrifuged at 100 rpm for 24 hours at room temperature using the Scorpion Scientific® A50651 apparatus until achieving complete hydration. Finally, the pH of each supernatant was measured via the Hanna Instruments® model HI3221 potentiometer.

2.5. Sorption Study.

Sorption experiments were carried out at 20°C. A standard stock solution of 1000 mg/L of aldrin was firstly prepared by dissolving the standard aldrin reagent (98.4% purity; from Chem Service®) in acetone; this solution was further diluted to the concentrations required for each experiment. The sorption experiments were carried out using a batch system at different concentrations (10 mg/L, 20 mg/L, 30 mg/L, 40 mg/L, 50 mg/L, 60 mg/L, 80 mg/L, 100 mg/L, 120 mg/L, 160 mg/L, 180 mg/L, and 200 mg/L), polypropylene tubes, and a ratio of 0.01 g of sorbent to 0.01 L of aqueous aldrin solution. It is important to note that the experiments were carried out in the dark in order to reduce the degradation process of the aldrin and favour the adsorption process. Each sample was stirred at 120 rpm for 24 hours; subsequently, the liquid phase was separated by centrifugation, 10 mL of hexane was added, and the solution was stirred manually for 10 minutes to extract the aldrin. Finally, the sample concentration was adjusted to 2 mL in the Buchi® R-300 rotary evaporator and later to 0.5 μL in the N$_2$ atmosphere. The analysis of the liquid phase was performed by gas chromatography/mass spectrometry with an Agilent® 6890N coupled to an Agilent® 5973 with an HP® 190915-433 capillary column.

3. Results and Discussion

3.1. Iron Nanoparticles (FeNPs).

The original FeNPs consisted of black fine powder, as observed in Figure 1(a) to avoid oxidation, and the FeNPs were washed with degassed ethanol several times and stored in an argon atmosphere. These FeNPs reacted to an external magnetic field, as shown in Figure 1(b), because of their ferromagnetic properties. These particles exhibit cooperative spin behaviour; i.e., the spins are oriented in the same direction within a section of the material called "the domain." By reducing nanoparticle sizes below a critical size, super-paramagnetism (SP) is established, in which the cooperative spin behaviour disappears, and the thermal energy is enough to destroy any such cooperative effect.

3.2. SEM and TEM Image Analyses of Materials.

Once the FeNPs were incorporated into the polymeric composite, a change in colour was observed. The Chi-EGDE-Fe beads were tinted in yellow (Figure 2(a)), which can be attributed to the oxidation of the FeNPs. In Figure 2(b), the average particle diameter of the composite was 2.64 mm. After the lyophilization process, the composite exhibited spherical particles had a rough structure and presented small channels on its surface (see Figure 2(c)). Zooming in 500x reveals that the channels have an almost pentagonal arrangement that is repeated, forming a honeycomb with thick contours that are about 10 μm thick, with a diameter close to 40 μm (see Figure 2(d)). In order to observe how the FeNPs were distributed within the spheres, a sphere was cut transversally and observed at 50x (see Figure 2(e)). It is observed from Figure 2(e) that the internal structure of a sphere has very small channels with an average diameter of 34 nm. Furthermore, they are, for the most part, distributed homogeneously but make up agglomerates in some regions with sizes up to 4.2 μm. Since the surfaces of these spherical particles are rough and porous, there are favourable transfers of mass and energy flows between the contaminant and the adsorbent material. The average pore diameter was 204 nm, classifying it as a macroporous material, whilst the pores with larger diameter were found on the surface, above 2.5 μm in depth [20]. Table 1 shows the elemental composition of a
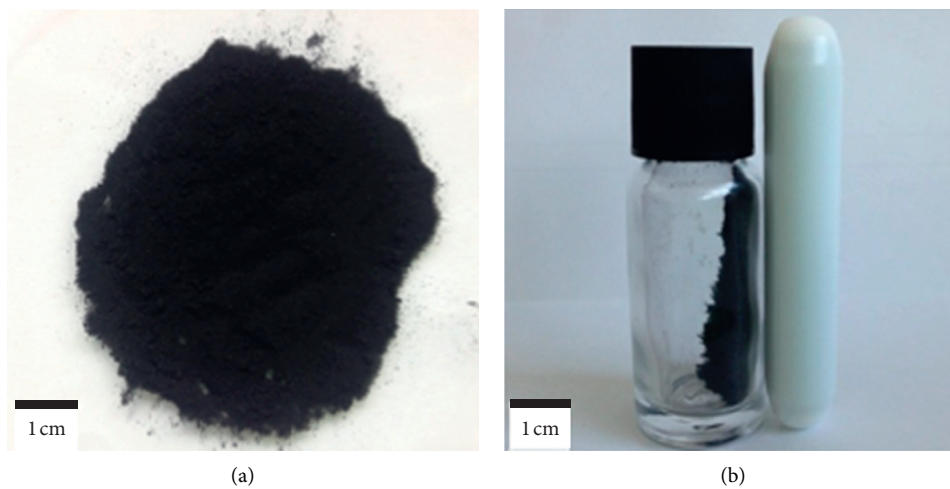
(a)

(b)

Figure 1: The FeNPs in (a) absence and (b) presence of an external magnetic field.
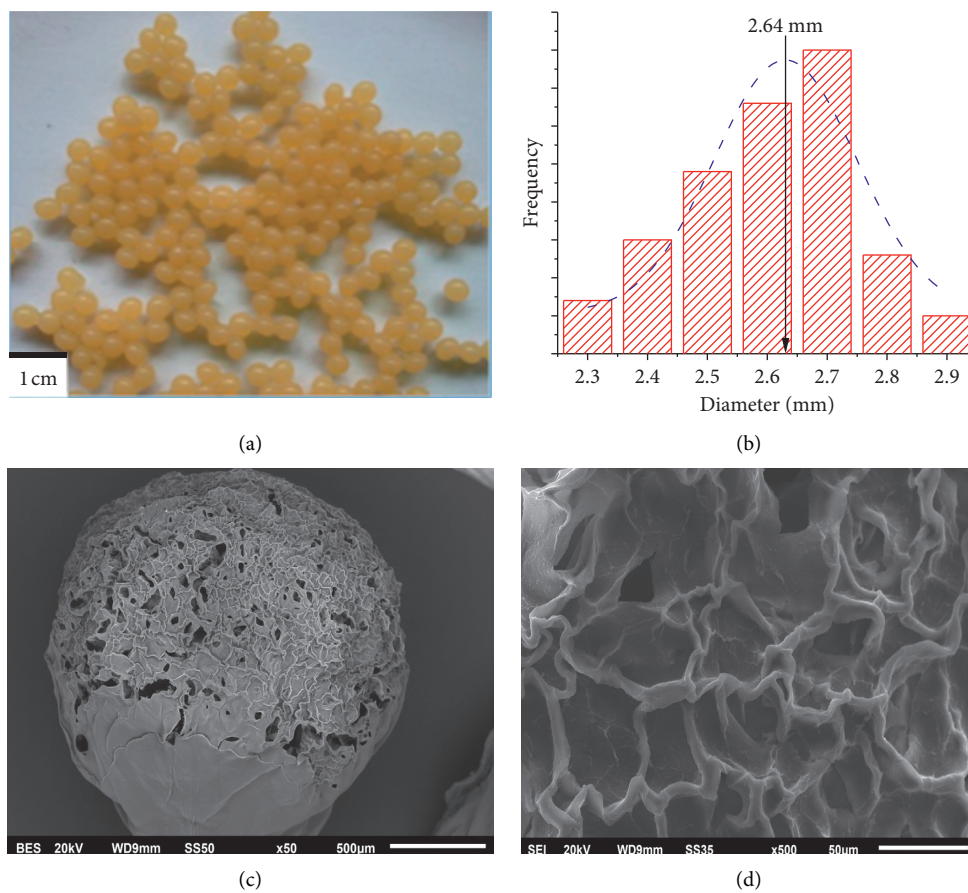

(a)

(b)

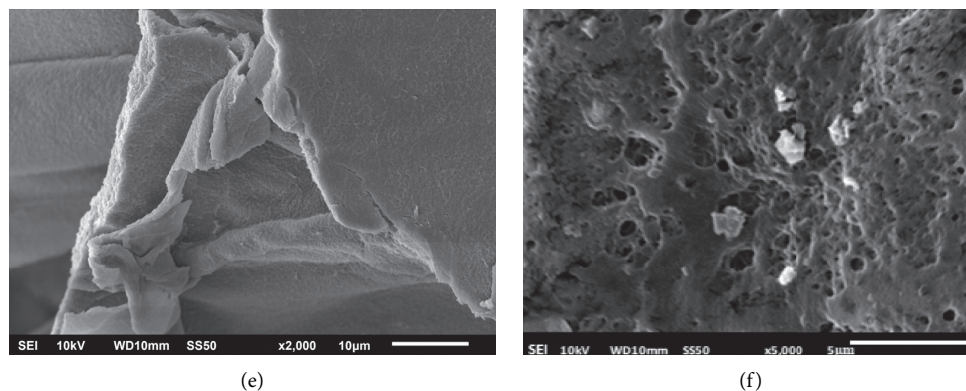
(c)

(d)

Figure 2: Continued.

(e)

(f)

FIGURE 2: (a) Chi-EGDE-Fe; (b) size of the bead; (c, d) SEM image of the external surface; (e, f) SEM image of the internal surface.

TABLE 1: Elemental analysis of Chi-EGDE-Fe beads.

| Element	Chi-EGDE-Fe % elemental
C	61.30
O	30.10
Al	0.44
Si	0.44
Cl	2.16
Fe	5.56

Chi-EGDE-Fe bead. The principal components are carbon and oxygen, which arise mainly from the chitosan and ethylene-glycol diglycidyl ether compounds. The addition of these latter substances resulted in a relatively low chlorine content that can be attributed to the chitosan. Small amounts of aluminum and silicon of unknown origin were also observed. Knidri et al. [21] noted the presence of silicon in chitosan spectra but failed to speculate on its origin. The presence of aluminum can be attributed to the sample holder since this device was made of aluminum. Finally, the Chi-EGDE-Fe beads had a small percentage of iron content.

TEM image processing was performed to measure the particle sizes of the FeNPs. Figure 3(a) shows spherical NPs forming long chains due to their strong magnetic nature; the measurements showed that the diameters were in the range of 10 nm to 50 nm, with an average diameter of 28 nm (see the inserted histogram in Figure 3(a)). When a close-up was made towards one of the nanoparticles (Figure 3(b)), a core-shell structure was observed with a core diameter of 17 nm and an external diameter of 25 nm, with the shells ranging in thickness from 2 nm to 4 nm. These core-shell particles are characteristic of FeNPs. When the FeNPs within the chitosan spheres were analyzed, it was observed that there were some morphological differences relative to those of the pure FeNPs. A thicker covering material surrounded these FeNPs, making it impossible to observe the core-shell structure. Inside the spheres, the particle diameters increased to ~70 nm. According to Chaudhuri [22] and Kopanja et al. [23], these types of clustered nanoparticles are typical after the stabilization process with chitosan has occurred.

3.3. Mössbauer Spectroscopy (MS).

Figure 4(a) shows the Mössbauer spectrum for the FeNPs, in which a superposition of three Mössbauer hyperfine patterns can be observed: two of magnetic and one of SP nature. The six-line magnetic pattern (green line) with a hyperfine magnetic field of $B = 33$ T is characteristic of metallic iron. The broader six-line magnetic pattern (blue line) with a hyperfine magnetic field of $B = 26$ T is characteristic of iron borides such as Fe_2B. Finally, the two-line quadrupole doublet (magenta line) can be associated with FeNPs having particle sizes below the 10 nm range. The hyperfine parameters of this quadrupole doublet, i.e., an isomer shift of $\delta = 0.34$ mm/s, a quadruple splitting of $\Delta E/2 = 0.75$ mm/s, and broad line widths of $\Gamma = 0.8$ mm/s, are typical of nanometric FeNPs including the shell materials composed of maghemite or magnetite [24]. When examining certain features of the Mössbauer spectra, it is possible to make some inferences about the particle sizes of the FeNPs. For example, if the Mössbauer spectrum of these FeNPs were to consist of broad and poorly resolved magnetic patterns, this pattern would be indicative of particles with sizes ranging between 12 nm and 15 nm; on the other hand, if a singlet or a doublet pattern were to be recorded, it would be indicative of particles with sizes <10 nm and in possession of super-paramagnetic properties. As the next section will show, the presence of maghemite/magnetite is further confirmed by XRD measurements on the unsupported FeNPs. On the other hand, Figure 4(b) shows the corresponding Mössbauer spectrum of the Chi-EDGE-Fe beads, which exhibits a quadrupole doublet only. The isomer shift (δ) and quadrupole splitting ($\Delta E/2$) parameters shown in Figure 4(b) are related to particles with sizes below the 10 nm range, as previously indicated; in this composite, it was not possible to detect the magnetic component of the FeNPs. In this particular case, the absence of magnetism may suggest that the FeNPs were totally oxidized during the synthesis of the Chi-EDGE-Fe beads. The FeNPs may have transformed into α-Fe_2O_3 particles of size <10 nm as a result of the synthesis of the composite, as inferred from the pale-yellow colour of the beads.
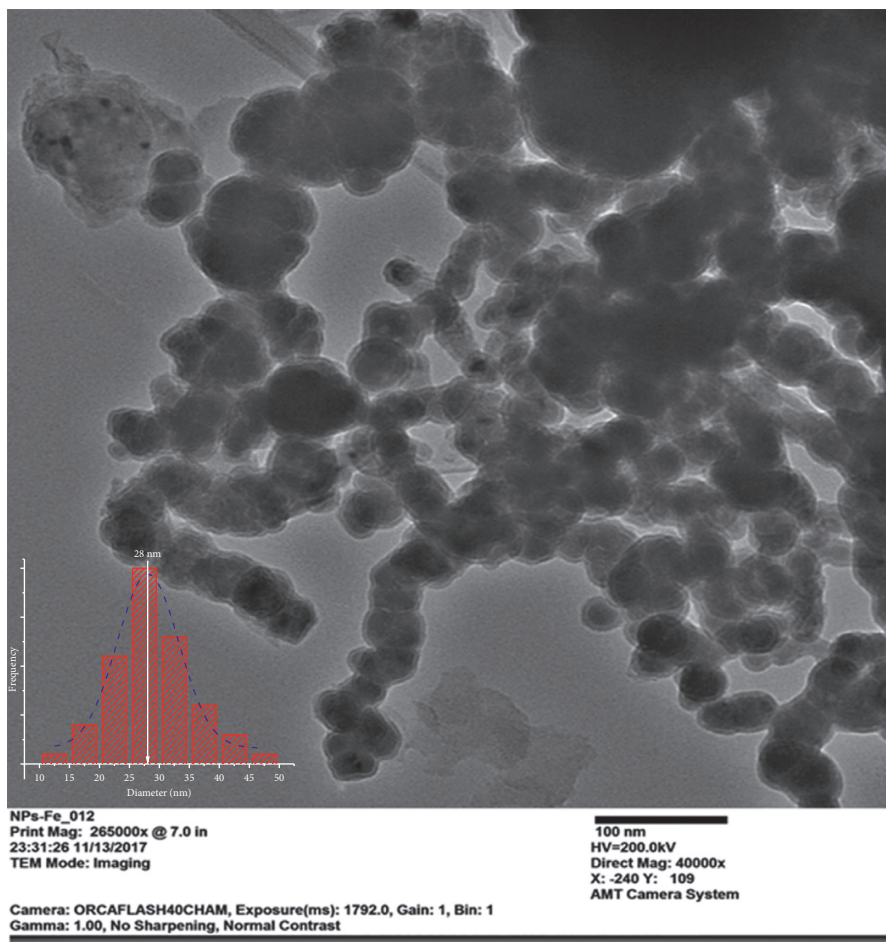
(a)
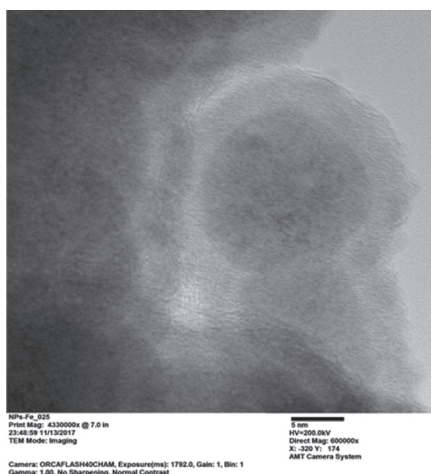
(b)
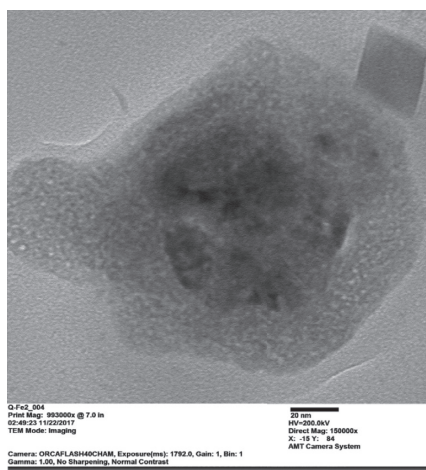
(c)

FIGURE 3: TEM: (a) fine particles of FeNPs; (b) ultrafine nanoparticles of FeNP core; (c) ultrafine nanoparticles of Chi-EGDE-Fe.

3.4. X-Ray Diffraction (XRD). The X-ray diffraction (XRD) analysis was conducted to investigate the crystalline structure of the FeNPs. Figure 5(a) shows the XRD patterns of these NPs, where the main diffracted lines, located at 35° and 45° in the 2θ° scale, indicate the presence of magnetite and metallic iron, respectively. Figures 5(b) and 5(c) show the XRD patterns of the Chi-EGDE and Chi-EGDE-Fe materials, respectively, with similar broad diffracted lines at ~10° and 20° and low intensities and broad signals between 35° and 40° on the 2θ scale. The broad, diffracted XRD lines of higher intensity are indicative of a low crystallization level for the chitosan, which is due to the low degree of
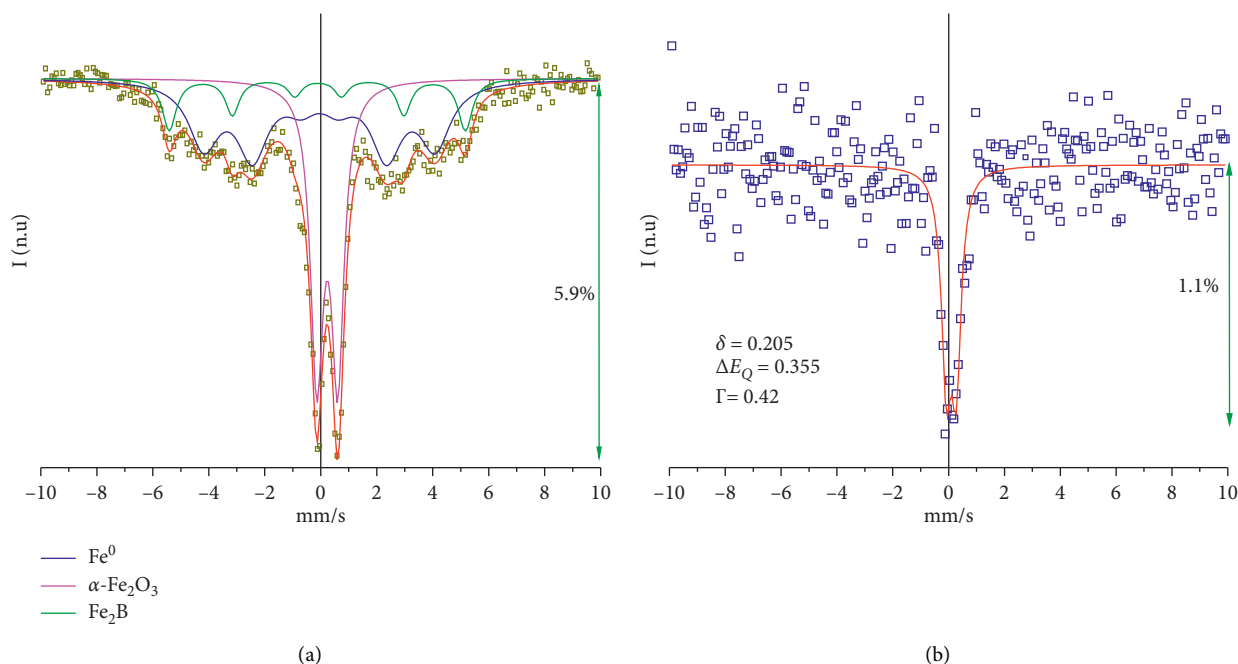
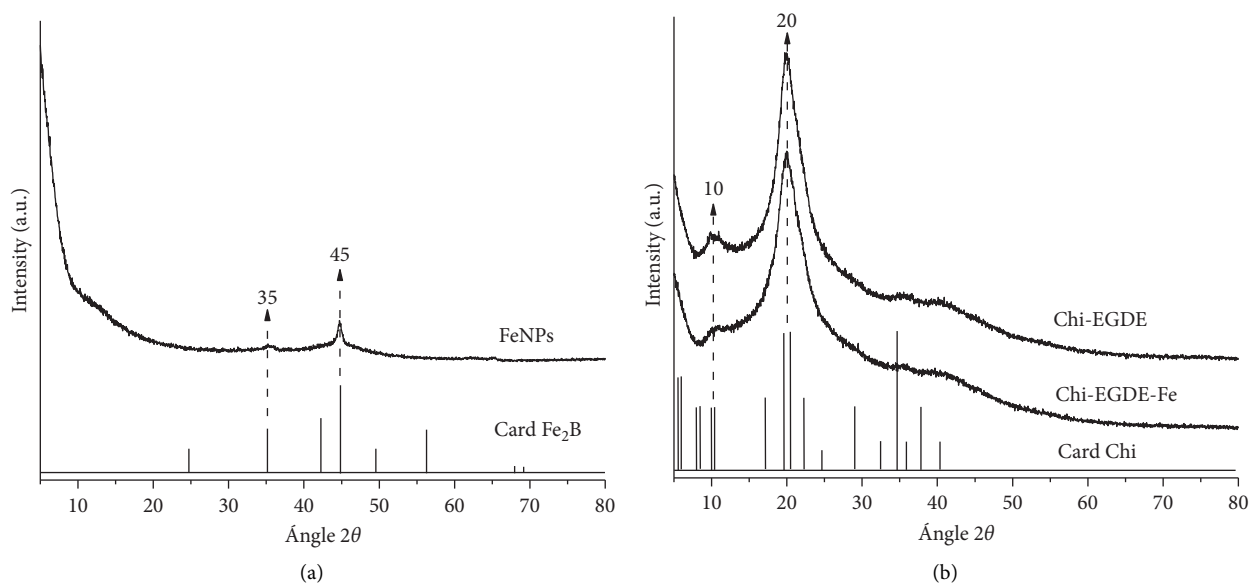FIGURE 4: Mossbauer spectra of (a) FeNPs and (b) Chi-EGDE-Fe.

FIGURE 5: XRD patterns of (a) FeNPs and (b) Chi-EGDE and Chi-EGDE-Fe.

deacetylation [25]. Ultrasmall hematite NPs could be suggested from the Mössbauer spectroscopy point of view, where the particles' size from 2 nm to 3 nm could be inferred [26]. However, neither the MS nor the XRD technique was able to discern the presence of hematite unambiguously. The inference was made based on the pale-yellow colour of the Chi-EGDE-Fe beads. The pure Chi-EGDE material was white. On the other hand, the hyperfine parameters of the quadrupole doublet in the composite were lower than those arising from the quadrupole doublet of the pure FeNPs

(Figure 4(a)), suggesting a different iron phase from those present in the pure FeNPs—the Fe° and Fe_2B, and phases and SP particles of maghemite/magnetite. The ambiguity in discerning the nature of the FeNPs in the composite arises from the fact that a very small amount of these FeNPs were mixed with the Chi-EGDE material to form the composite. A black or grey colour would be expected for the Chi-EGDE-Fe beads if no oxidation were to take place when this composite was produced. Instead, a pale-yellow colour was observed (Figure 2(a)). Thus, at this point in the analysis, the nature of

the iron NPs in the composite remained uncertain. To clear this point up, a 77 K Mössbauer spectrum would be required to search for the hyperfine magnetic field associated with the quadrupole doublet shown in Figure 4(b).

3.5. FTIR Analysis.

Figure 6 shows the FTIR spectra of the cross-linked Chi-EGDE-Fe beads. The broad peak located the ranges of 3600 cm^{-1} and 3100 cm^{-1} which corresponds to the overlapping stretching vibrations of N-H and O-H bonds [27]. The band at 2870 cm^{-1} can be assigned to symmetric and asymmetric stretching vibrations of the C-H bond of the methylene group CH$_2$. The band at 1647 cm^{-1} is the result of the flexion of the N-H bonds in the primary amino groups, and the band at 1424 cm^{-1} can be assigned to the flexural vibration of the amino groups C-N and N-H. Additionally, the band at 1376 cm^{-1} can be assigned to the C-O stretching vibration of a primary alcohol group, and the band at 1065 cm^{-1} corresponds to the free amino group [28]. Sathya et al. [29] reported that the peaks located at 610 cm^{-1} and 560 cm^{-1} are due to the formation of iron-oxide nanoparticles, whereas Iovescua et al. [30] reported that the peaks at 563 cm^{-1} and 461 cm^{-1} are characteristic of the stretching modes of Fe-O bonds in hematite. Several changes are observed in the FTIR spectrum after the sorption process in Chi-EGDE-Fe-aldrín material and in the functional groups corresponding to OH, N-H, C-N, and Fe-O, which indicate that these changes are directly related to the absorption of aldrin. The small shifts and intensity changes observed at approximately 1700 cm^{-1} to lower wavenumbers are probably related to the interactions between the amino groups and Cl ions of aldrin. Also, an interaction between the iron NPs and aldrin is noticeable in the 700 cm^{-1} and 500 cm^{-1} range.

3.6. Surface Characterization.

The specific surface area (SBET), volume, and pore diameter results for the Chi-EGDE-Fe beads and the FeNPs are shown in Table 2. The FeNPs have the greatest specific surface areas, with an average value of 44°m2/g$^{\circ}$ ± $^{\circ}$2 m^2/g; this value is similar to the one reported by Picasso et al. [31] and lower than that reported by Akhgar et al. [32]. These differences are attributed to the particle sizes of the FeNPs. On the contrary, the Chi-EGDE-Fe beads have a lower average specific surface area. This difference in specific surface area can be attributed to the FeNPs that are supported on the Chi-EGDE beads. As reported previously, the Fe content in the Chi-EGDE-Fe beads is only 5.56%, and this Fe is probably in the form α-Fe$_2$O$_3$, differing from the original FeNPs. It is important to note that the other parameters, namely, the TPV and APD, do not change appreciably between samples (Table 2).

The measured active site density for the Chi-EGDE-Fe beads was 28 sites/nm^2, and the isoelectric point was established at pH = 7. Hence, it is possible to infer that the surface of the material is positively charged. This condition favours the removal of molecules in a negatively charged solution. At pH > 6.92 and pH = 7, the surfaces of the Chi-EGDE-Fe beads would be negatively charged in such a way
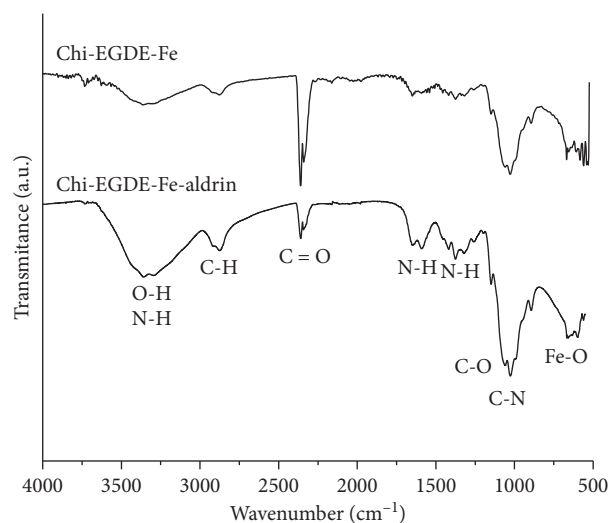

FIGURE 6: FTIR spectra.

these materials would not be able to remove organic compounds.

3.7. Sorption Isotherm as a Function of Aldrin Concentration.

The sorption of aldrin by means of the Chi-EGDE-Fe beads under equilibrium conditions (q_e), as a function of the aldrin concentration (C_e), is presented below. The sorption process took place at 20°C whilst using a contact time of 24 hours and several aldrin concentrations. The experimental data were fitted to the mathematical models developed by Langmuir, Freundlich, and Langmuir–Freundlich, and the best fit was obtained with the Langmuir–Freundlich model. The maximum adsorption capacity of the beads reached 74.84 mg/ g$^{\circ}$ ± $^{\circ}$2 mg/g. Figure 7 shows the fitted experimental data using the Langmuir–Freundlich model only, which is expressed in equation (1) below. Langmuir–Freundlich isotherm includes the knowledge of adsorption heterogeneous surfaces. It describes the distribution of adsorption energy onto heterogeneous surface of the adsorbent [33]. At a low adsorbate concentration, this model becomes the Freundlich isotherm model, whilst at a high adsorbate concentration, it becomes the Langmuir isotherm. Langmuir–Freundlich isotherm can be expressed as follows:

$$q_e = \frac{q_{MLF} \left(K_{LF} C_e \right)^{M_{LF}}}{1 + \left(K_{LF} C_e \right)^{M_{LF}}}. \tag{1}$$

Here, q_e (mg/g) is the amount of the sorbed adsorbate under equilibrium conditions, q_{MLF} is the maximum adsorption capacity (mg/g−1), K_{LF} is equilibrium constant for heterogeneous solid, and MLF is heterogeneous parameter. These parameters can be obtained by using the nonlinear regression techniques. The calculated isothermal coefficients are summarized in Table 3.

3.8. Proposed Removal Mechanism.

The interaction between the aldrin and the Chi-EDGE-Fe can occur in two possible ways, with the first way being a sorption process

TABLE 2: Specific surface area, volume, and pore size parameters of the studied materials.

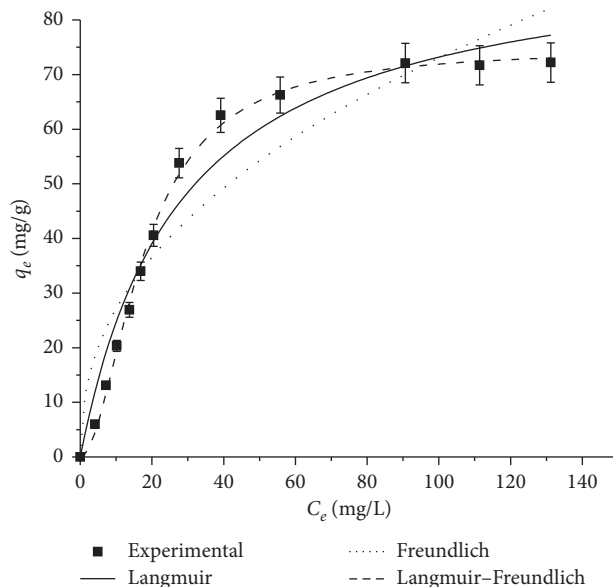| Material	SBET (m^2/g)	Total pore volume (TPV) (cm^3/g)	Average pore diameter (APD) (nm)
FeNPs	44.20	0.19	17.10
Chi-EGDE-Fe	38.91	0.17	17.08

FIGURE 7: Fitting data of the isotherm points to Langmuir, Freundlich, and Langmuir–Freundlich model.

TABLE 3: Adjustment parameters for Langmuir, Freundlich, and Langmuir–Freundlich models.

Model	Equation	Settings
Langmuir	$q_e = q_0 b c_2 / (1 + b c_2)$	$R_2 = 0.97$ $q_o = 93.69$ mg g^{-1} $b = 0.04$ L mg^{-1}
Freundlich	$q_e = K_F C_e^{1/n}$	$R^2 = 0.90$ $K_F = 10.04$ mg g^{-1} $n = 2.32$
Langmuir–Freundlich	$q_e = q_{MLF} (K_{LF} C_e)^{M_{LF}} / (1 + (K_{LF} C_e)^{M_{LF}})$	$R^2 = 0.99$ $q_{MLF} = 74.84$ mg g^{-1} $K_{LF} = 0.0047$ L mg^{-1} $M_{LF} = 1.86$

and the second one involving a degradation process. The adsorption mechanism can involve a physical entrapment or a chemical binding via weak Van der Waals forces, dipole-dipole and ion-dipole interactions, cation exchanges, strong covalent bonding, and a physisorption, which could take place in multiple layers [34, 35]. Figure 8 shows the proposed sorption mechanism for the interaction between Chi-EGDE-Fe and aldrin developed by the Avogadro Vision 1.2.0 software. In the FTIR analysis, it was possible to observe several active sites, including hydroxyl (OH) and amino (NH) groups, as well as C-O and Fe-OH bonds, on the surface of the composite, all of which favour the adsorption of aldrin. The sorption of aldrin can be carried out via different mechanisms, one of which involves the C-OH sites and

aldrin-Cl bonds, whilst another one involves the Fe-OH groups and aldrin-Cl ions. The FTIR analysis appears to indicate that all these interactions occur because several frequency shifts of these functional groups were observed. This observation coincides with the sorption isotherm fitted with the Langmuir–Freundlich model, considering that, in this work, the sorption process is carried out at high concentrations and the adsorbate is sorbed at sites located in fixed positions and may be arranged in a monolayer form; in this case, all the sites are energetically equivalent. Is important to note that a diffusion of aldrin molecules into the primary porous structure of the Chi-EDGE-Fe seems to be impossible, so only the active surface sites of the secondary porosity structure may be accessible for the diffusion and
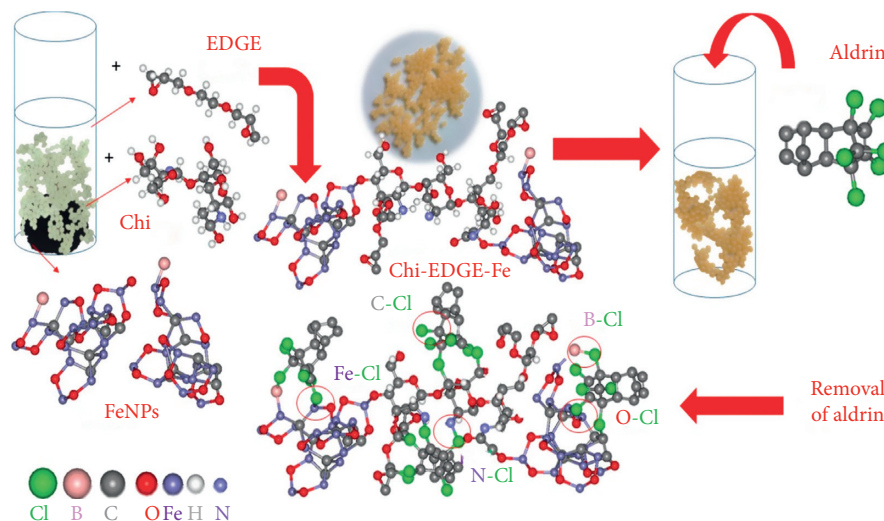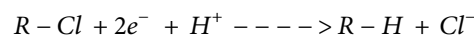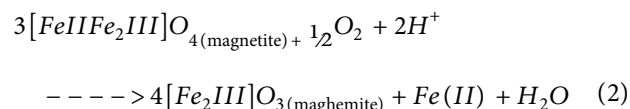
FIGURE 8: Proposal mechanism between Chi-EGDE-Fe and the aldrin.

adsorption of the pesticide molecules. Thus, the degradation of aldrin cannot be ruled out given the presence of iron-oxide NPs; in this case, hematite NPs are highly reactive with crystal defects, such as vacancies, which are unstable electrostatic points and act on any substance having dipolar properties. Using the present results, it is not possible to distinguish between a sorption and degradation process for aldrin. Thus, both the sorption and degradation of aldrin may occur. The sorption process may occur through electrostatic interactions caused by the inductive effect of the chlorine atoms in aldrin, and the functional groups in the composite may influence the degradation process through the crystal defects in the hematite NPs.

However, several studies support the degradation of aldrin. Shoiful et al. [13] show that, in the absence of sunlight, aldrin degradation occurs after 12 hours and that this process is strongly influenced by the dissociation energy of C-Cl bonding within the structure [36]. The degradation products of aldrin have not been identified experimentally as of yet. However, these degradation products have been predicted with computation models [37], which indicate that aldrin undergoes degradation to form dieldrin and pentachlordieldrin. Bandala et al. [38] indicate, however, that the degradation process can produce low yields due to the hydrophobic character of aldrin. Sayles et al. [39] explain that the degradation of aldrin with Fe^0 NPs begins when iron-oxides form on the surfaces of the nanoparticles in the aqueous phase, resulting in magnetite (Fe_3O_4) that contains Fe^{2+} groups, which then initiate the degradation reaction that results in

the formation of free radicals [40]. The reaction is described as follows:

$$3[FeIIFe_2III]O_{4(magnetite)} + \tfrac{1}{2}O_2 + 2H^+$$

$$---->4[Fe_2III]O_{3(maghemite)} + Fe(II) + H_2O \quad (2)$$

$$R - Cl + 2e^- + H^+ ---->R - H + Cl^-$$

According to Yamada [36], in this process, the H^+ plays an important role in the dissociation of magnetite and reduction of aldrin. In this particular case, this mechanism is ruled out due to the absence of magnetite. The results of the current study were compared with the data concerning the sorption of aldrin on different adsorbents (Table 4). It was noted that our nanoparticle beads of chitosan-Fe (Chi-EGDE-Fe beads) showed the best results for the sorption of aldrin. Furthermore, Lu et al. [8] prepared a compound of chitosan beads, used them for aldrin removal, and reported a low sorption capacity compared to the present work. Sprynsky et al. [34] utilized clinoptilolite and reported 4.99 μg/g of aldrin removal. Also, Bakouri et al. [41] reported 19.54 mg/g of aldrin removal using acid-treated olive stones as an adsorbent. Thus, nanoparticle beads of chitosan-Fe exhibited an acceptable performance in comparison to these other adsorbents. This situation can be explained by the formation of surface sites and the specific area that provides the increase in the adsorption capacity to remove aldrin in solution.

TABLE 4: Works with chitosan and/or iron particles.

Adsorbent material	Pollutant	Maximum removal capacity	References
Clinoptilolite	Aldrin	4.99 (μg/g)	[34]
Acid-treated olive stones	Aldrin	19.54 (mg/g)	[41]
Chitosan beads	Aldrin	2 (ng/g)	[8]
Bacterial cells	Aldrin	20 (ng/g)	[42]
Biomimetic absorbent	Aldrin	0.89 (μg/g)	[43]
Cellulose acetate (CA) embedded with triolein (CA-triolein)	Aldrin	4 (mg/g)	[44]
Q-Fe	Aldrin	74.84 (mg/g)	This work

4. Conclusion

In the present work, FeNPs were synthesized by means of the chemical reduction method and were supported in chitosan beads cross-linked with ethylene glycol diglycidyl ether (Chi-EGDE-Fe). The supporting strategy was used in order to improve the handling and recovery of the FeNPs in the sorption of aldrin in aqueous media. Three iron phases, namely, Fe^0, Fe_3O_4, and Fe_2B, were identified in the unsupported black FeNPs. The FeNPs had a core-shell type structure, with the core consisting of Fe^0 or Fe_2B and having a diameter of ~28 nm, and the shell of magnetite being ~2–4 nm thick. The chitosan-EGDE-supported FeNP beads were pale-yellow in colour, had a spherical form, and were of high roughness. The iron in these beads was possibly in hematite form. The FTIR spectrum showed a noticeable difference in the interval from $500\,cm^{-1}$ to $700\,cm^{-1}$, due to the interaction with Chi-EDGE-Fe-aldrin. As a result of the analysis of the aldrin sorption isotherms, a maximum sorption capacity of 74.84 mg/g ± 2 mg/g was obtained for the iron beads. The experimental data fit the Langmuir–Freundlich model better (with a correlation of 0.99), indicating that, in the sorption process, a single layer of the pollutant may be formed on the surface of the adsorbent material. The interactions between Chi-EGDE-Fe and aldrin could take place on the available active sites on the surfaces of the beads, as such between C-OH and Cl and Fe-OH and Cl. The degradation process of aldrin may have occurred through a reductive process triggered by the crystal defects in the hematite NPs.

Data Availability

The data used to support the findings of this study are available from the corresponding author upon request.

Additional Points

(i) We obtained beads of chitosan-ethylene glycol diglycidyl ether combined with iron-nanoparticles.(ii) To adsorb aldrin from aqueous effluents. (iii) Depending on the concentration, the percentage of aldrin removed changes. (iv) The Langmuir–Freundlich model described the aldrin isothermal sorption on the material.

Conflicts of Interest

The authors declare that they have no conflicts of interest.

References

[1] K. Deering, E. Spiegel, C. Quaisser et al., "Exposure assessment of toxic metals and organochlorine pesticides among employees of a natural history museum," *Environmental Research*, vol. 184, 2020.

[2] S. N. Khuman, P. G. Vinod, G. Bharat, Y. S. M. Kumar, and P. Chakraborty, "Spatial distribution and compositional profiles of organochlorine pesticides in the surface soil from the agricultural, coastal and backwater transects along the south-west coast of India," *Chemosphere*, vol. 254, 2020.

[3] G. Shukla, A. Kumar, M. Bhanti, P. E. Joseph, and A. Taneja, "Organochlorine pesticide contamination of ground water in the city of Hyderabad," *Environment International*, vol. 32, no. 2, pp. 244–247, 2006.

[4] M. Anand and A. Taneja, "Organochlorine pesticides residue in placenta and their influence on anthropometric measures of infants," *Environmental Research*, vol. 182, pp. 1–6, 2020.

[5] E. A. Moawed and A. M. Radwan, "Application of acid modified polyurethane foam surface for detection and removing of organochlorine pesticides from wastewater," *Journal of Chromatography B*, vol. 1044-1045, pp. 95–102, 2017.

[6] X. Jin, Y. Liu, X. Qiao et al., "Risk assessment of organochlorine pesticides in drinking water source of the Yangtze river," *Ecotoxicology and Environmental Safety*, vol. 182, p. 109390, 2019.

[7] C. J. Martyniuk, A. C. Mehinto, and N. D. Denslow, "Organochlorine pesticides: agrochemicals with potent endocrine-disrupting properties in fish," *Molecular and Cellular Endocrinology*, vol. 507, p. 110764, 2020.

[8] L. C. Lu, C. I. Wang, and W. F. Sye, "Applications of chitosan beads and porous crab shell powder for the removal of 17 organochlorine pesticides (OCPs) in water solution," *Carbohydrate Polymers*, vol. 83, no. 4, pp. 1984–1989, 2011.

[9] M. J. García-Galán, L. S. Monllor-Alcaraz, C. Postigo et al., "Microalgae-based bioremediation of water contaminated by pesticides in peri-urban agricultural areas," *Environmental Pollution*, vol. 265, p. 114579, 2020.

[10] C. M. Dominguez, N. Oturan, A. Romero, A. Santos, and M. A. Oturan, "Optimization of electro-Fenton process for effective degradation of organochlorine pesticide lindane," *Catalysis Today*, vol. 313, pp. 196–202, 2018.

[11] L. A. Abron and J. O. Osburn, "A transport mechanism in hollow nylon fiber reverse osmosis membranes for the

removal of ddt and aldrin from water," *Water Research*, vol. 7, no. 3, pp. 461–477, 1973.

[12] R. A. Farghali, M. Sobhi, S. E. Gaber, H. Ibrahim, and E. A. Elshehy, "Adsorption of organochlorine pesticides on modified porous Al30/bentonite: kinetic and thermodynamic studies," *Arabian Journal of Chemistry*, vol. 13, no. 8, pp. 6730–6740, 2020.

[13] A. Shoiful, Y. Ueda, R. Nugroho, and K. Honda, "Degradation of organochlorine pesticides (OCPs) in water by iron (Fe)-based materials," *Journal of Water Process Engineering*, vol. 11, pp. 110–117, 2016.

[14] M. O. Munyati, A. Mbozi, and M. N. Siamwiza, "Polyaniline nanoparticles for the selective recognition of aldrin: synthesis, characterization, and adsorption properties," *Synthetic Metals*, vol. 233, pp. 79–85, 2017.

[15] I. Diale, A. Galdames, M. L. Alonso, L. Bartolomé, J. L. Vilas, and R. M. Alonso, "Effect of coating on the environmental applications of zero valent iron nanoparticles: the lindane case," *Science of the Total Environment*, vol. 565, pp. 795–803, 2016.

[16] W.-C. Tsai, M. D. G. de Luna, H. L. P. Bermillo-Arriesgado et al., "Competitive fixed-bed adsorption of Pb(ii), Cu(ii), and Ni(ii) from aqueous solution using chitosan-coated bentonite," *International Journal of Polymer Science*, vol. 2016, pp. 1–11, 2016.

[17] H. E. Ramírez-Guerra, F. J. Castillo-Yañez, E. A. Montaño-Cota et al., "Protective effect of an edible tomato plant extract/chitosan coating on the quality and shelf life of sierra fish fillets," *Journal of Chemistry*, vol. 2018, pp. 1–6, 2018.

[18] C. Luk, J. Yip, C. Yuen, C. Kan, and K. Lam, "A comprehensive study on adsorption behaviour of direct, reactive and acid dyes on crosslinked and non-crosslinked chitosan beads," *Journal of Fiber Bioengineering and Informatics*, vol. 7, no. 1, pp. 35–52, 2014.

[19] L. C. Bell, A. M. Posner, and J. P. Quirk, "The point of zero charge of hydroxyapatite and fluorapatite in aqueous solutions," *Journal of Colloid and Interface Science*, vol. 42, no. 2, pp. 250–261, 1973.

[20] D. H. Everett, "Manual of symbols and terminology for physicochemical quantities and units appendix II: definitions, terminology and symbols in colloid and surface chemistry," *IUPAC Pure and Applied Chemistry*, vol. 31, no. 4, pp. 577–638, 1972.

[21] H. Knidri, R. Khalfaouy, A. Laajeb, A. Addaou, and A. Lahsini, "Eco-friendly extraction and characterization of chitin and chitosan from the shrimp shell waste via microwave irradiation," *Process Safety and Environmental Protection*, vol. 104, pp. 395–405, 2016.

[22] S. Chaudhuri, "Core/shell nanoparticles: classes, properties, synthesis mechanisms, characterization, and applications," *Chemical Reviews*, vol. 112, pp. 2373–2433, 2012.

[23] L. Kopanja, S. Kralj, D. Zunic, B. Loncar, and M. Tadic, "Core-shell superparamagnetic iron oxide nanoparticle (SPION) clusters: TEM micrograph analysis, particle design and shape analysis," *Ceramics International*, vol. 42, no. 9, pp. 10976–10984, 2016.

[24] M. Siddique, E. Ahmed, and N. M. Butt, "Particle size effect on Mössbauer parameters in γ-Fe2O3 nanoparticles," *Physica B: Condensed Matter*, vol. 405, no. 18, pp. 3964–3967, 2010.

[25] H. El Knidri, J. Dahmani, A. Addaou, A. Laajeb, and A. Lahsini, "Rapid and efficient extraction of chitin and chitosan for scale-up production: effect of process parameters on deacetylation degree and molecular weight," *International Journal of Biological Macromolecules*, vol. 139, pp. 1092–1102, 2019.

[26] E. M. Kutashova, A. V. Pyataev, N. F. Shkodich, A. S. Rogachev, and Y. B. Scheck, "Fe-B nanomaterials by mechanochemical synthesis: a Mössbauer study," *Journal of Magnetism and Magnetic Materials*, vol. 492, p. 165663, 2019.

[27] T. C. Sunarti, M. I. Febrian, E. Ruriani, and I. Yuliasih, "Some properties of chemical cross-linking biohydrogel from starch and chitosan," *International Journal of Biomaterials*, vol. 2019, pp. 1–6, 2019.

[28] S. Subramani and N. Thinakaran, "Isotherm, kinetic and thermodynamic studies on the adsorption behaviour of textile dyes onto chitosan," *Process Safety and Environmental Protection*, vol. 106, pp. 1–10, 2017.

[29] K. Sathya, R. Saravanathamizhan, and G. Baskar, "Ultrasound assisted phytosynthesis of iron oxide nanoparticle," *Ultrasonics Sonochemistry*, vol. 39, pp. 446–451, 2017.

[30] A. Iovescu, G. Stînğă, M. E. Maxim et al., "Chitosan-poly-glycidol complexes to coating iron oxide particles for dye adsorption," *Carbohydrate Polymers*, vol. 246, p. 116571, 2020.

[31] G. Picasso, J. Vega, R. Uzuriaga, and G. Ruiz, "Preparación de nanopartículas de magnetita por los métodos sol-gel y precipitación: estudio de la composición química y estructura," *Revista de la Sociedad Química del Perú*, vol. 78, pp. 170–182, 2012.

[32] B. N. Akhgar and P. Pourghahramani, "Implementation of sonochemical leaching for preparation of nano zero-valent iron (NZVI) from natural pyrite mechanochemically reacted with Al," *International Journal of Mineral Processing*, vol. 164, pp. 1–5, 2017.

[33] N. Ayawei, A. N. Ebelegi, and D. Wankasi, "Modelling and interpretation of adsorption isotherms," *Journal of Chemistry*, vol. 2017, pp. 1–11, 2017.

[34] M. Sprynsky, T. Ligor, and B. Buszewski, "Clinoptilolite in study of lindane and aldrin sorption processes from water solution," *Journal of Hazardous Materials*, vol. 151, pp. 570–577, 2008.

[35] M. N. Rashed, "Adsorption technique for the removal of organic pollutants from water and wastewater," in *Organic Pollutants: Monitoring, Risk and Treatment*, M. N. Rashed, Ed., IntechOpen, London, UK, 2013.

[36] S. Yamada, Y. Naito, M. Funakawa, S. Nakai, and M. Hosomi, "Photodegradation fates of cis-chlordane, trans-chlordane, and heptachlor in ethanol," *Chemosphere*, vol. 70, no. 9, pp. 1669–1675, 2008.

[37] U. Schenker, M. Scheringer, and K. Hungerbuhler, "Including degradation products of persistent organic pollutants in a global multi-media box model," *Environmental Science Pollution Research*, vol. 14, p. 145, 2007.

[38] E. R. Bandala, S. Gelover, M. T. Leal, C. Arancibia-Bulnes, A. Jimenez, and C. A. Estrada, "Solar photocatalytic degradation of aldrin," *Catalysis Today*, vol. 76, no. 2-4, pp. 189–199, 2002.

[39] G. D. Sayles, G. You, M. Wang, and M. J. Kupferle, "DDT, DDD, and DDE dechlorination by zero-valent iron," *Environmental Science & Technology*, vol. 31, no. 12, pp. 3448–3454, 1997.

[40] E. M. Rodríguez, G. Fernández, P. M. Álvarez, R. Hernández, and F. J. Beltrán, "Photocatalytic degradation of organics in water in the presence of iron oxides: effects of pH and light source," *Applied Catalysis B: Environmental*, vol. 102, no. 3-4, pp. 572–583, 2011.

[41] H. El Bakouri, J. Usero, J. Morillo, and A. Ouassini, "Adsorptive features of acid-treated olive stones for drin pesticides:

equilibrium, kinetic and thermodynamic modeling studies," *Bioresource Technology*, vol. 100, pp. 4147–4155, 2009.

[42] I. C. Mac Rae, "Removal of chlorinated hydrocarbons from water and wastewater by bacterial cells adsorbed to magnetite," *Water Research*, vol. 20, no. 9, pp. 1149–1152, 1986.

[43] H. Liu, J. Qu, R. Dai, J. Ru, and Z. Wang, "A biomimetic absorbent for removal of trace level persistent organic pollutants from water," *Environmental Pollution*, vol. 147, no. 2, pp. 337–342, 2007.

[44] H. Liu, J. Ru, J. Qu, R. Dai, Z. Wang, and C. Hu, "Removal of persistent organic pollutants from micro-polluted drinking water by triolein embedded absorbent," *Bioresource Technology*, vol. 100, no. 12, pp. 2995–3002, 2009.